Effect of geotextile reinforcement on soil-steel flexible bridges

Mohamed E. El-Naggar and Baha Eldin El-Sharnouby
Civil Eng. Dept., Faculty of Engineering, Alexandria University, Alexandria, Egypt

Finite element technique was employed to investigate the improvement in load-carrying capacity of soil-steel bridge due to the presence of geotextile. Soil-steel bridges are those bridges, which are comprised of structural steel plates and engineered soil, designed and constructed to induce a beneficial interaction of the two materials. The load effects in a soil-steel bridge depend upon various factors, such as the geometry of the structure, dispersion of the concentrated loads through the backfill, the material properties of the metallic shell and those of the surrounding soil. This paper focuses on the analysis and design of multi-layered reinforced soil-steel bridges with geotextile.

يستخدم مبدأ زيادة جساءة التربة باضافة المكونات المختلفة لها في العديد من المجالات التطبيقية، فهي تستخدم في زيادة قوة تحمل التربة الضعيفة واتزان الميول والعديد من التطبيقات الأخرى. وتستخدم الالواح المعدنية المرنة علي هيئة مواسير او الواح متعرجة منحنية بالتداخل مع التربة لانشاء الكباري فوق مجاري المياه او الطرق الصغيرة. إلا أن تصميم هذه الكباري المزدوجة من التربة والواح المعدنية تحكمها مواصفات وكودات لم تأخذ في الاعتبار إمكانية زيادة اتزان هذه المنشآت عن طريق زيادة جساءة التربة بالأنسجة التسليحية. وفي هذا البحث تمت دراسة مدي تأثير استخدام الانسجة التسليحية في زيادة كفاءة تلك الكباري وذلك نظريا بتوظيف متقدم بطريقة العناصر المتناهية في الصغر. اربعة عناصر مختلفة من تلك العناصر تم استخدامها لتمثيل كلا من التربة والواح الكوبري والانسجة التسليحية واسطح التقابل بينهم. وقد خلص البحث الي توضيح اهمية تسليح التربة بالانسجة والذي يؤثر بكفاءة قد تصل الي ٣٠% من قدرة الكوبري بدون تسليح للتربة المحيطة به. ويقدم البحث ايضا مجموعة من المعادلات المباشرة التي يمكن عن طريقها حساب الاجهادات في جسم الكوبري المزدوج من التربة والواح الصلب المرن مع الاخذ في الاعتبار تأثير تسليح التربة.

Keywords: Soil-steel structures, Geotextile, Soil reinforcements, Load-carrying capacity, Traffic load

1. Introduction

Soil reinforcement is one of the most common civil engineering applications of geotextile [1-5]. Soil-steel bridges are tremendously used around the world [6-9]. The North America design codes; such as: Ontario Highway Bridge Design Code, (OHBDC) [10] and American Association of State Highway and Transportation Officials, (AASHTO) [11] have not included the effects of using geotextile layers placed within the backfill soil around and over the wall of soil-steel bridge. In the analysis of these structures, the effect of axial forces is usually considered ignoring the effect of bending moments [8]. As well known, reinforcement increases the load-carrying capacity of soil and hence increases the modulus of subgrade reaction of soil [1,2,4]. Increasing the modulus of subgrade reaction leads to decrease the stresses induced in corrugated flexible steel plates of soil-steel bridges. Due to this reduction in steel plates, thinner plates can be used and more economy can be achieved. Design analysis of soil-steel bridges ranges between extremely easy to apply empirical design methods and fairly complex methods involving the use of finite element analysis [6-9]. This study presents the contribution of geotextile reinforcements on the stability of soil-steel bridges. Finite element method was employed to study the effect of geotextile to increase the load-carrying capacity of soil-steel bridges. Bending moments, axial forces and deflections at different positions of the corrugated flexible steel bridges with and without the use of geotextile were calculated due to the effect of both backfill and traffic loads. The results were verified with the results obtained by the Ontario design code method and the AASHTO design code method for unreinforced structures. An extensive parametric study is conducted to examine the behavior of the structures with and without reinforcement. The parameters varied included: the span of bridge, the height

© Faculty of Engineering Alexandria University, Egypt.

of cover over the bridge crown and the modulus-area of the geotextile. Design formulas for obtaining the internal forces induced in the wall of soil-steel bridges, including the pertaining parameters are proposed.

2. Geometry of the structure

Fig. 1 illustrates the geometry of the cross-section of soil-steel bridge used in the analysis. The depth of cover over the bridge crown, *H*, is chosen to varying from tenth of the span, *S*, to the span width. The extension of backfill around the bridge is chosen to be equal half the bridges span to covering the requirements of the Ontario Highway Bridge Design Code, (OHBDC). The bedding thickness under the bridge can be estimated using the bearing capacity analysis, which shows that it is usually less than the bridge span, *S*. Bridge span, *S* is the width of the opening, fig. 1.

3. Theoretical background

Ontario Highway Bridge Design Code, (OHBDC) and American Association of State Highway and Transportation Officials, (AASHTO) are the most specific design methods related to the analysis of soil-steel bridges. These methods concerned with the analysis of unreinforced soil-steel system and they required some specified conditions to be valid, such as the minimum depth of cover, the spacing between conduits, and the extent of backfill soil around the structure.

3.1. Ontario code method (OHBDC)

For the design of soil-steel bridges, the OHBDC design method requires only the consideration of ultimate limit state under one loading including combination of dead and live loading including the effect of impact. This code also requires that consideration be given only to the thrust in the conduit wall, with bending moments in it being neglected.

3.2. Dead load thrust

The thrust, T_D in the conduit wall is assumed to have the same value all round the conduit, it is obtained from:

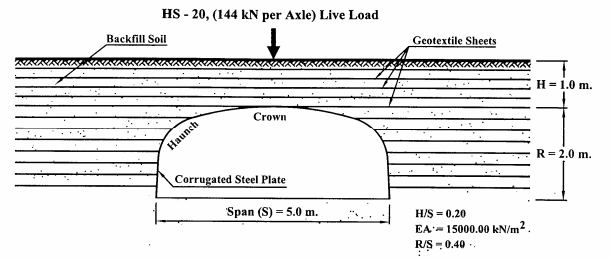

Fig. 1. Geometry of soil-steel bridge. (Example of case study).

$$T_D = 0.5(1.0-0.1C_s)\, A_f\, W. \quad (1)$$

In which W is the weight of fill directly above the conduit per unit length, A_f is a coefficient depending upon the depth of cover and the shape of the conduit, and C_s is a dimensionless parameter defining the relative axial rigidity of the conduit wall with the soil stiffness as:

$$C_s = (E_s^*/E_c)\,(D_v/A). \quad (2)$$

In which E_c is the modulus of elasticity of conduit wall material, E_s^* is the effective secant modulus of soil, which may be taken as:

$$E_s^* = E_s/(1-\nu^2). \quad (3)$$

In which E_s is the Young's modulus of soil, D_v is the rise of the conduit and ν is the Poisson's ratio of soil.

3.3. Live load thrust

The thrust T_L is also assumed to have the same value all round the conduit, it is obtained from:

$$T_L = 0.5\,\sigma_L\, m_f\,(1.0+DLA)\,*(\text{leaser of } D_h \text{ and } L_t). \quad (4)$$

In which σ_L is the equivalent uniform distributed load at the crown level, which is obtained by assuming that the wheel loads at the embankment level are distributed through the fill at an angle of 45° in the transverse direction of the conduit and at a slope of one horizontally to two vertically in the longitudinal direction, m_f is the modification factor to

account for multilane loading, which is equal to 1.0, 0.9, 0.8, and 0.7 for 1, 2, 3, and 4 loaded lanes, *DLA* is the dynamic load allowance and L_t is the length of the dispersed load at the crown level.

3.4. Minimum depth of cover

To get valid results by using the OHBDC design method, the minimum depth of cover over the conduit crown should be the largest of the following:

$(D_h / 6)(D_h / D_v)^{0.5}$ or $0.4(D_h / D_v)^2$ *or 0.60 m.*

Where D_h is the conduit span.

3.5. Minimum extent of backfill

The backfill must be extent to at least half the conduit span D_h to covering the requirements of the OHBDC design method.

4. American association of state highway and transportation code method

The AASHTO specifications permit both the working-stress and load-factor design method. Similarly to the OHBDC, the AASHTO design code emphasized that the only design force effect on the wall is the axial force without any effect of the bending moments.

4.1. Conduit wall thrust

The conduit wall thrust T_l is calculated by using the ring compression theory and it can be obtained from:

$$T_l = 0.5\{\alpha_D P_D + \alpha_L (1.0 + DLA) P_L\} D_h. \quad (5)$$

Where P_D and P_L are the nominal equivalent uniformly distributed pressures at the crown level due to the soil dead load and live load, respectively, α_D and α_L are dead and live loads factors, being effectively 1.95 and 2.171, respectively, and *DLA* is the impact factor.

The pressure P_D is the free-filed overburden pressure at the crown level, which can be obtained from:

$$P_D = \gamma H. \quad (6)$$

Where γ is the soil density and H is the depth of cover.

The equivalent live load pressure P_L is calculated by assuming, that a wheel load of the HS-20 vehicle is uniformly distributed over a square area each side equals 1.75 times the depth of cover. This procedure is applicable only when $H > 2$ *ft* (0.61 m).

5. Material properties

The soils used in this study are Well-graded coarse-grained soils compacted to a minimum of 90% standard proctor density. It, also, assumed to be homogenous, at least over the bridge crown, H and around the bridge to at least over a distance equal to half the bridge span, S. The dry unit weight, γ_d, of these soils is taken to be equal 18.0 kN/m^3, and the angle of internal friction, ϕ, is taken to be 30^o.

The mechanical properties of the geotextile used in this work are defined by its modulus-area, *EA*, in which A is the cross-sectional area of geotextile and E is the modulus of elasticity of geotextile. The modulus-area of the geotextile is ranged from 0.10 to 100000. The geotextile layers arranged within the cover and around the bridge in even space.

Corrugated steel plates are used to represent the bridge wall. The properties of these plates are, the area of cross section = 6.771 mm^2/m, the second moment of inertia of the cross-sectional area = 2079.8 mm^4/m and the modulus of elasticity of the used material = 2.0x10^5 MPa.

Because dual-axle trucks are the common vehicles used in the design of soil-steel bridges, the AASHTO HS-20 dual-axle truck is adopted throughout this work.

6. Theoretical model

Two-dimensional finite element technique was adopted throughout this analysis. Fig. 2 illustrates the finite element mesh implemented in the analysis. Four types of elements were employed to describe the structure (fig. 3). Soil elements were represented by plane-strain eight-node bilinear elements. Bridge wall elements were idealized by linearly

elastic three-node beam elements. Geotextile elements were modeled by using three-node truss elements with no compressive strength. A nonslip three-node per side interface element was induced with the finite element description to treat the interface between geotextile and soil elements and between the bridge wall and soil elements. The boundary conditions imposed were (i) the base nodes located on the base line AB were restrained in the horizontal and vertical directions; and, (ii) the side nodes located on the right and left vertical end zones were not allowed to move horizontally.

6.1. Representation of traffic load

Since the two-dimensional analysis is adopted in this analysis, the traffic load must be represented in two-dimensional. The two-dimensional analysis represents a slice of unit thickness through the bridge wall and the backfill. It assumes that the slice analyzed is representative of any section along the length

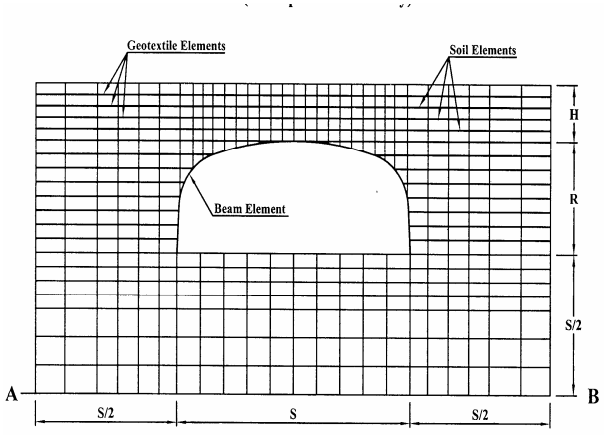

Fig. 2. Finite element mesh.

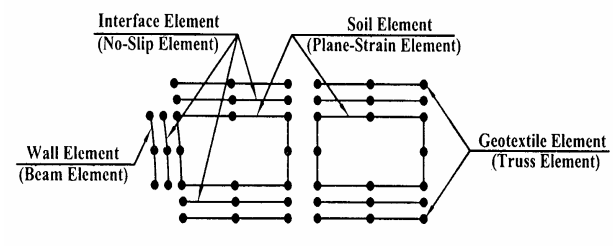

Fig. 3. Types of finite elements used.

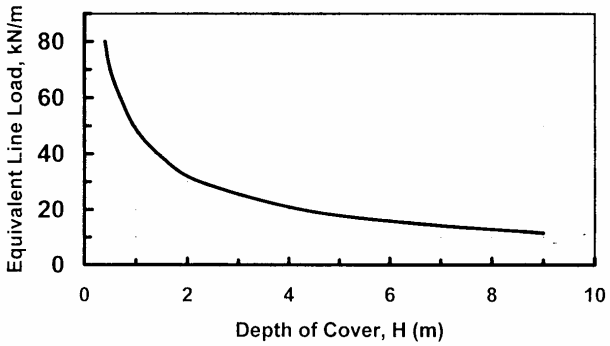

Fig. 4. Effective live load pressure at the crown level recommended by AASHTO.

of the structure and that loads are continuous along this length of the structure. Therefore, to perform two-dimensional analyses of the HS-20 AASHTO load effects, it is necessary to represent its actual load by an equivalent line loading which is continuous along the length of the structure. Fig. 4 represents the equivalent line load of the HS-20 truck, which recommended by the AASHTO specifications. The line load obtained from this figure produces the same peak vertical stress at the crown of the structure as the actual traffic load produces.

7. Results

7.1. Bending moments

Figs. 5 and 6 illustrate the distribution of bending moments induced in the bridge wall with and without the use of geotextile under the effect of backfill load and the effect of both backfill and traffic loads. The results showed that the reduction in the maximum bending moment value due to the use of geotextile was about 22% at the bridge crown and was about 20% at the bridge haunch due to the effect of backfill. But in case of load from backfill and traffic loads, the reduction in bending moment due to the use of geotextile was about 12% at the bridge crown and about 17% at the bridge haunch. This reduction takes place due to the friction stresses created at soil-geotextile interfaces, which tend to confine the soil around the bridge and consequently decrease the bending moment in the bridge cross-section.

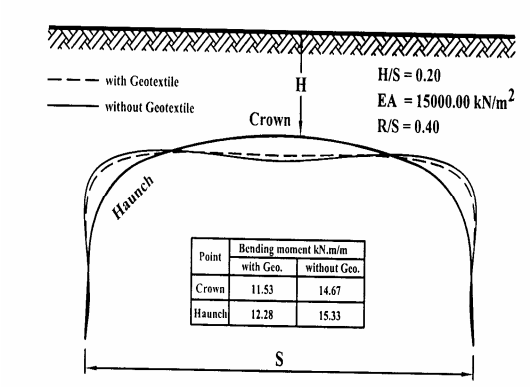

Point	Bending moment kN.m/m	
	with Geo.	without Geo.
Crown	11.53	14.67
Haunch	12.28	15.33

Fig. 5. Bending moment distribution due to backfill load.

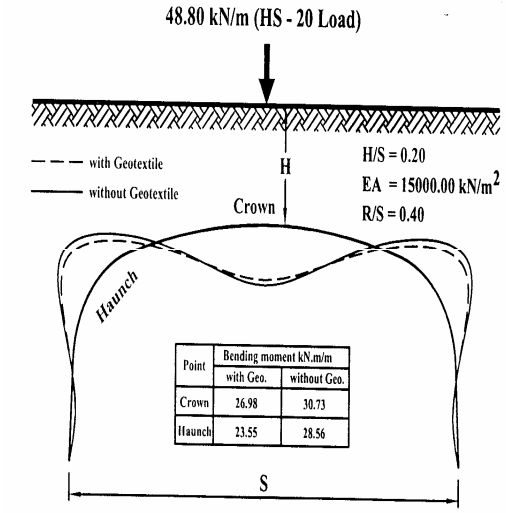

Point	Bending moment kN.m/m	
	with Geo.	without Geo.
Crown	26.98	30.73
Haunch	23.55	28.56

Fig. 6. Bending moment distribution due to backfill and traffic loads.

7.2. Axial forces

The distribution of axial forces induced in the bridge wall was determined with and without the geotextile under backfill load and under both backfill and traffic loads, figs. 7 and 8. The results showed an increase of the maximum crown and haunch axial forces. Comparing with unreinforced backfill, the maximum crown axial force was increased by about 23% and the maximum haunch axial force was increased by about 14% under the effect of backfill load. A similar phenomenon was observed at the maximum crown or haunch axial force under the effect of backfill and traffic loads, fig. 8. This increase occurred due to the contribution of geotextile, which tend to increase the horizontal stiffness of the geotextile-soil system. Increasing the horizontal stiffness of the structure tends to increase the shear stresses at geotextile-soil interface and thus, increases the horizontal stresses induced in the bridge cross-section.

7.3. Crown deflections

Crown deflections were greatly affected by the use of geotextile. A significant reduction in the crown deflection was obtained due to the contribution of geotextile, figs. 9 and 10. The reduction was about 28% due to the effect of backfill only and was about 23% due to the effect of both backfill and traffic loads. This reduction in crown deflection is a direct result from the reduction in the bending moments.

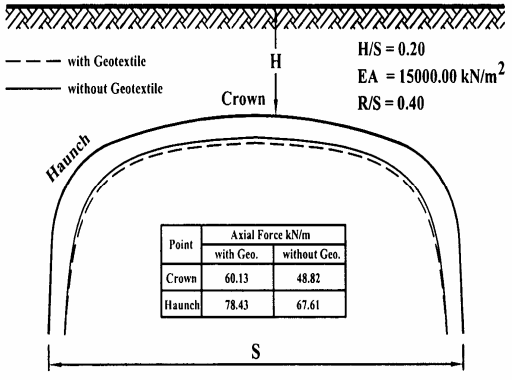

Point	Axial Force kN/m	
	with Geo.	without Geo.
Crown	60.13	48.82
Haunch	78.43	67.61

Fig. 7. Axial force distribution due to backfill load.

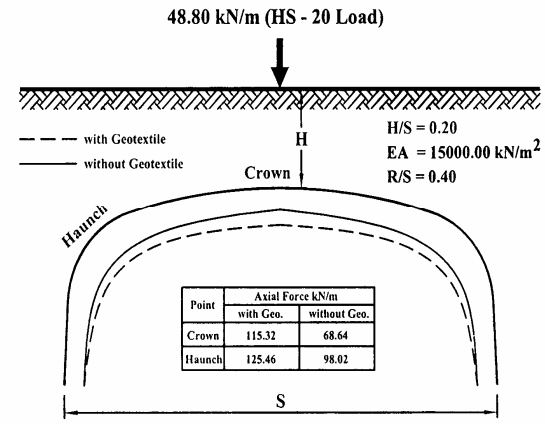

Point	Axial Force kN/m	
	with Geo.	without Geo.
Crown	115.32	68.64
Haunch	125.46	98.02

Fig. 8. Axial force distribution due to backfill and traffic loads.

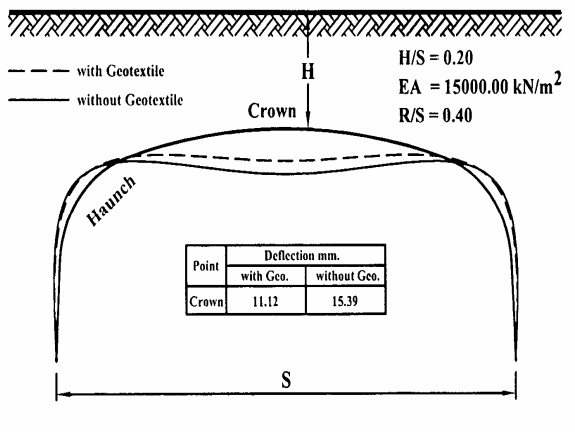

Fig. 9. Deflection due to backfill load.

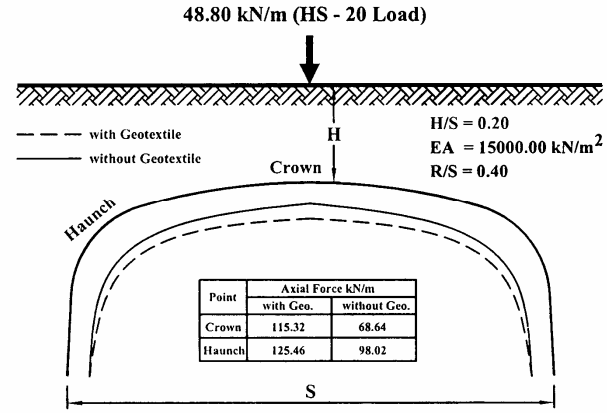

Fig. 10. Deflections due to backfill and traffic loads.

8. Parametric study

The parametric study conducted in this work includes the following design parameters: the modulus-area of geotextile, *EA*; the rise-to-span ratio, *R/S*; and the height of cover-to-span ratio, *H/S*.

8.1. Modulus-area of geotextile

Figs. 11 and 12 illustrate the variation of crown bending moment ratios, m_{cb} and m_{ct}, for a wide range of the modulus-area of geotextile, *EA* due to the effect of backfill and traffic loads, respectively. Where: $m_{cb}= M_{cb}/(\gamma*H*S^2)$ and $m_{ct}= M_{ct}/(P_a*S)$. For a rise-to–span ratio, *R/S*=0.40 and a height of cover-to-span ratio, *H/S*=0.20, the relationship shows a linear trend on semi-logarithmic scale.

From figs. 11 and 12, the crown bending moment ratio due to the effect of backfill load and the effect of traffic load, m_{cb}, m_{ct}, can be expressed as:

$$m_{cb} = [344 - 9.3\ ln(EA)]/\ 1000\ , \quad (7)$$

and

$$m_{ct} = [25 - 0.013\ ln(EA)]/\ 1000. \quad (8)$$

The sum of eqs. (7) and (8) gives the crown bending moment ratio, m_c due to the effect of both backfill and traffic loads as:

$$m_c = m_{cb} + m_{ct}\ . \quad (9)$$

Figs. 13 and 14 represent the variation of haunch bending moment ratios, m_{hb} and m_{ht} for a wide range of the modulus-area of geotextile, *EA* due to the effect of backfill and

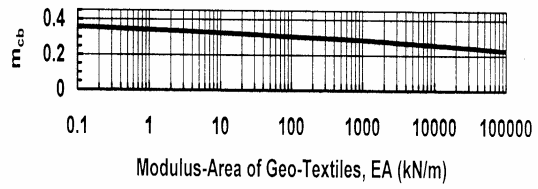

Fig. 11. Crown bending moment ratio, m_{cb} versus m dulus-area of geo-textiles, *EA* due to backfill load.

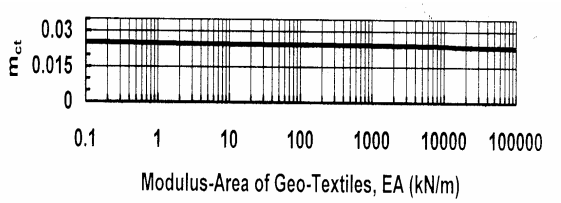

Fig. 12. Crown bending moment ratio, m_{cb} versus modulus-area of geo-textiles, *EA* due to traffic load.

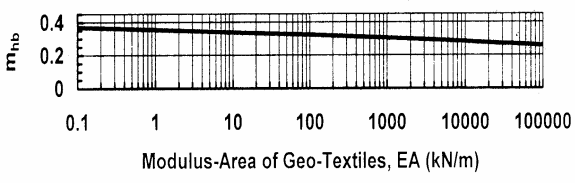

Fig. 13. Haunch bending moment ratio, m_{hb} versus modulus-area of geo-textiles, *EA* due to backfill load.

traffic loads, respectively. Where: $m_{hb}= M_{hb}/(\gamma *H*S^2)$ and $m_{ht}= M_{ht}/(P_a*S)$. For the case of R/S=0.40 and H/S=0.20, the variation of results shows a linear relationship on semi-logarithmic scale.

From fig. 13, the haunch bending moment due to the effect of backfill load, m_{hb} can be obtained from:

$$m_{hb} = [357 - 8.2\ ln(EA)]/1000. \quad (10)$$

The above equation becomes:

$$m_{ht} = [19.6 - 0.29\ ln(EA)]/1000\ . \quad (11)$$

When the traffic load is applied, fig. 14.

The sum of eq. (10) and eq. (11) gives the haunch bending moment ratio, m_h due to the effect of both backfill and traffic loads as:

$$m_h = m_{hb} + m_{ht}\ . \quad (12)$$

Figs. 15 and 16 represent the variation of crown axial force ratios, t_{cb} and t_{ct} for different values of the modulus-area of geotextile, EA due to the effect of backfill and traffic loads,

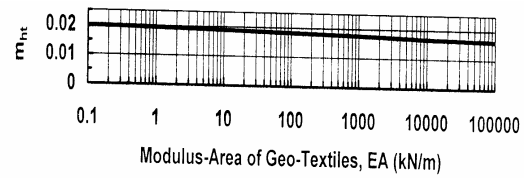

Fig. 14. Haunch bending moment ratio, m_{bt} versus modulus-area of geo-textiles, EA due to backfill load.

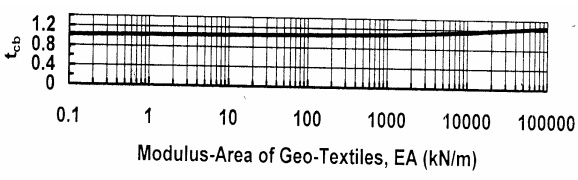

Fig. 15. Haunch bending moment ratio, m_{hb} versus modulus-area of geo-textiles, EA due to backfill load.

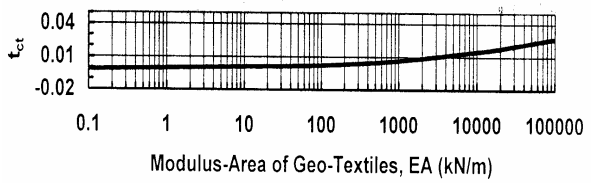

Fig. 16. crown axial force ratio, t_{ct} versus modulus-area of geo-textiles, EA due to traffic load.

respectively. In which $t_{cb} = T_{cb}/(\gamma*S^2)$ and $t_{ct} = T_{ct}/(P_a*S)$. For R/S=0.40 and H/S=0.20, the relationship shows a linear trend on semi-logarithmic scale.

From the best fit of the plot in fig. 15, the crown axial force ratio due to the effect of backfill load, t_{cb} may be expressed as:

$$t_{cb} = [1022 + 15\ ln(EA)]/1000. \quad (13)$$

Also based on the plotted results in fig. 15, the crown axial force ratio due to the effect of traffic load, t_{ct} is given by:

$$t_{ct} = [-\ 1.66 + 1.89\ ln(EA)]/1000\ . \quad (14)$$

The sum of eq. (13) and eq. (14) gives the crown axial force ratio, t_c due to the effect of both backfill and traffic loads as:

$$t_c = t_{cb} + t_{ct}\ . \quad (15)$$

Figs. 17 and 18 illustrate the relation between the crown axial force ratios, t_{hb} and t_{ht} for a wide range of the modulus-area of geotextile, EA due to the effect of backfill and traffic loads, respectively. In which: $t_{hb}= T_{hb}/(\gamma*S^2)$ and $t_{ht}= T_{ht}/(P_a*S)$. For R/S=0.40 and H/S=0.20, the results showed a linear relationship on semi-logarithmic scale.

From figs. 17 and 18, the haunch axial force ratio due to the effect of backfill load and the effect of traffic load, t_{hb}, t_{th} can be expressed as:

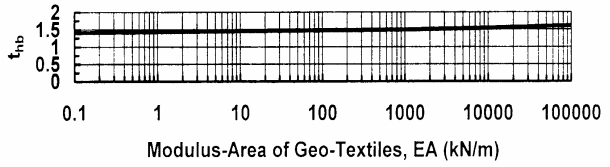

Fig. 17. Haunch axial force ratio, t_{hb} versus modulus-area of geo-textiles, EA due to traffic load.

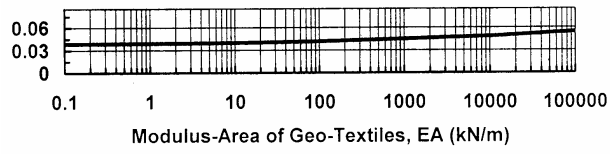

Fig. 18. Haunch axial force ratio, t_{ht} versus modulus-area of geo-textiles, EA due to traffic load.

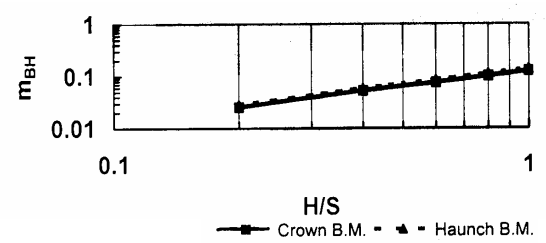

Fig. 19. Haunch axial force ratio, t_{hb} versus modulus-area of geo-textiles, EA due to traffic load.

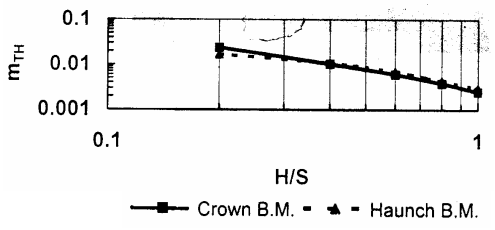

Fig. 20. Relation between $Ln\ (m_{TH})$ and log (H/S) due to traffic load.

$$t_{hb} = [1425 + 13.5\ ln(EA)]/1000, \quad (16)$$

and

$$t_{ht} = [38.91 + 1.10\ ln(EA)]\ /1000\ . \quad (17)$$

The sum of eq. (16) and eq. (17) gives the haunch axial force ratio, t_h due to the effect of both backfill and traffic loads as:

$$t_h = t_{hb} + t_{ht}\ . \quad (18)$$

8.2. Height-to-span ratio

Fig. 19 illustrates the relation between the height-to-span ratio, H/S and the crown and haunch bending moments ratios due to the effect of backfill when the rise-to-span ratio, R/S= 0.40, and the modulus-area of geotextile, EA =15000.0 kN/m. The relationship shows a linear trend on logarithmic scale and a very close result for both crown and haunch bending moment ratios. From the best fit of this plot, the crown or haunch bending moment ratio due to the effect of backfill, m_{bH} may be expressed as:

$$m_{bH} = 5.0\ x\ m_b\ x\ (H/S)^{0.98}\ . \quad (19)$$

Fig. 20 presents the relation between the height-to-span ratio, H/S and the crown and haunch bending moments ratio due to the effect of traffic load when the rise-to-span ratio, R/S= 0.40, and the modulus-area of geotextile, EA = 15000.0 kN/m. The results from this figure show a very close result for both crown and haunch bending moment ratios. As well as, a linear trends when the logarithmic scale is used. From this chart, the crown or haunch bending moment ratio due to the effect of traffic load, m_{tH} may be given from the following form:

$$m_{tH} = 0.15\ x\ m_t\ x\ (H/S)^{1.25}\ . \quad (20)$$

Fig. 21 demonstrates the relation between the height-to-span ratio, H/S and the crown and haunch axial force ratios due to the effect of backfill, t_{bH}. For R/S= 0.40, and EA= 15000.0 kN/m, the relationship shows a linear trend on logarithmic scale with a very little difference between the crown and the haunch axial force ratios. From the best fit of this plot, the crown or haunch axial force ratio due to the effect of backfill, t_{bH} may be estimated as:

$$t_{bH} = 4.50\ x\ t_b\ x\ (H/S)^{0.95}. \quad (21)$$

Fig. 22 illustrates the variation of crown and haunch axial force ratio, t_{tH} for a wide range of the height-to-span ratio, H/S, when the rise-to-span ratio, R/S= 0.40, and the modulus-area of geotextile, EA=15000.0 kN/m. The relationship shows a linear trend on logarithmic scale. From this plot, the crown or haunch axial force ratio due to the effect of traffic load, t_{tH} may be taken from:

$$t_{tH} = 0.25\ x\ t_t\ x\ (H/S)^{0.92}. \quad (22)$$

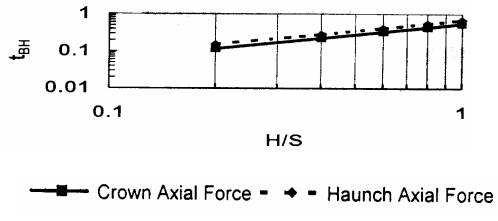

Fig. 21. Relation between $Ln\ (t_{BH})$ and $Ln\ (H/S)$ due to backfill load.

8.3. Rise-to-span ratio

Fig. 23 illustrates the relation between the rise-to-span ratio, R/S and the crown and haunch bending moments ratio due to the effect of backfill when the height-to-span ratio, H/S=0.20, and the modulus-area of geotextile, EA=15000.0 kN/m. The results obtained show a very close result for both crown and haunch bending moment ratios, m_{bR} and a linear trend on logarithmic scale. From the best fit of this plot, the crown or haunch bending moment ratio, m_{bR} may be expressed as:

$$m_{bR} = 0.70 \times m_{bH} \times (R/S)^{-0.40}. \quad (23)$$

Fig. 24 presents the relation between the rise-to-span ratio, R/S and the crown and haunch bending moments ratio due to the effect of traffic load when the height-to-span ratio, H/S= 0.20, and the modulus-area of geotextile, EA = 15000.0 kN/m. The results from this figure show a linear trend when the logarithmic scale is used. From this chart, the crown or haunch bending moment ratio, m_{tR} may be given from:

$$m_{tR} = 0.62 \times m_{tH} \times (R/S)^{-0.51}. \quad (24)$$

Fig. 25 demonstrates the relation between the rise-to-span ratio, R/S and the crown and haunch axial force ratio due to the effect of backfill under the following conditions: a) the height-to-span ratio, H/S= 0.20, and b) the modulus-area of geotextile, EA = 15000.0 kN/m. The results obtained show a very little difference between the crown and the haunch axial force ratios and a linear trend on logarithmic scale. From the best fit of this plot, the crown or haunch axial force ratio, t_{bR} may be estimated as:

$$t_{bR} = 1.07 \times t_{bH} \times (R/S)^{0.15} \quad . \quad (25)$$

Fig. 26 illustrates the relation between the rise-to-span ratio, R/S and the crown and haunch axial force ratio due to the effect of

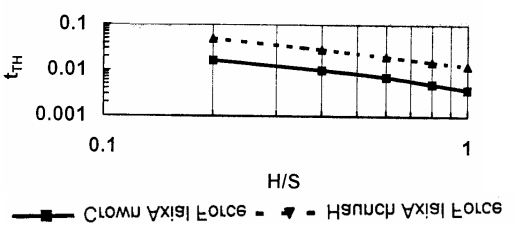

Fig. 22. Relation between *Ln* (t_{TH}) and *Ln* (H/S) due to traffic load.

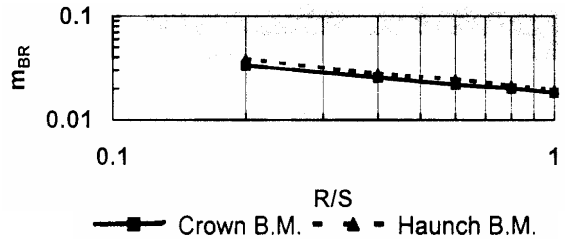

Fig. 23. Relation between *Ln* (m_{BR}) and *Ln* (R/S) due to backfill load.

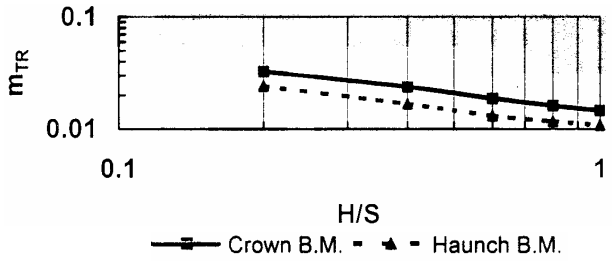

Fig. 24. Relation between *Ln* (m_{TR}) and *Ln* (R/S) due to traffic load.

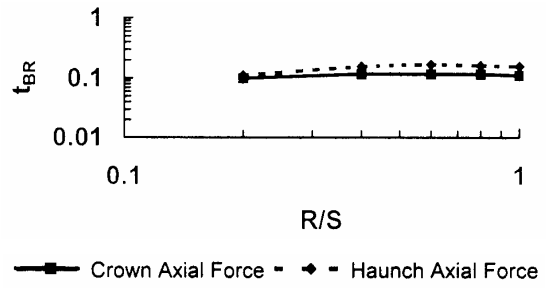

Fig. 25. Relation between *Ln* (t_{BR}) and *Ln* (H/S) due to backfill load.

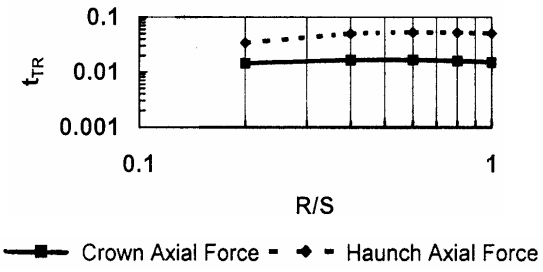

Fig. 26. Relation between *Ln* (t_{TR}) and *Ln* (H/S) due to traffic load.

traffic load when the height-to-span ratio, H/S= 0.20, and the modulus-area of geotextile, EA = 15000.0 kN/m. The results demonstrate a little change between the crown and the haunch axial force ratios with the same slope of the best-fit line. From this plot, the crown or haunch axial force ratio due to the effect of traffic load, t_{tR} may be taken from:

$$t_{tR} = 1.03 \times t_{tH} \times (R/S)^{0.05}. \quad (26)$$

Eqs. (23) to (26) are general formulas to evaluate the internal forces induced in the bridge wall at its crown or haunch points due to different parameters.

9. Conclusions

This study presents the contribution of geotextile reinforcements on the stability of soil-steel bridges. Reinforced and unreinforced structures are studied. The OHBDC and the AASHTO design code methods were taken as a guide for the basic cases of the unreinforced backfill. Results showed a significant reduction in the bending moment at both the crown and haunch of the bridge wall due the geotextile as well as an increase of the maximum crown and haunch axial force. Reduction in crown deflection occurs when using geotextile due to the increase of backfill stiffness. Formulas showing the variation in internal forces induced in the cross-section of soil-steel bridge with the pertaining parameters are proposed. These formulas are valid for the range of parameters used in this analysis.

Notations

A cross-sectional area of geotextile,
A_f coefficient depending on the depth of cover and the shape of the conduit,
C_s dimensionless parameter,
D bedding thickness,
D_h conduit span,
D_v rise of the conduit,
DLA dynamic load allowance,
E modulus of elasticity of geotextile,
E_c modulus of elasticity of conduit wall material,
E_s Young's modulus of soil,
E_s* effective secant modulus of soil,
EA modulus-area of the geotextile,
H depth of cover,
L_t length of the dispersed load at the crown level,
m_f modification factor,
m_c Crown bending moment ratio,
m_{cb} crown bending moment ratio due to backfill only,
m_{ct} crown bending moment ratio due to traffic load,
m_c crown bending moment ratio due to the effect of backfill and traffic loads,
m_{hb} haunch bending moment ratio due to backfill,
m_{ht} haunch bending moment ratio due to traffic load,
m_h haunch bending moment ratio due to the effect of backfill and traffic loads,
m_{bH} crown or haunch bending moment ratio due to the effect of backfill for different values of height-to-span ratio,
m_{bR} crown or haunch bending moment ratio due to the effect of backfill for different values of rise-to-span ratio,
m_{tH} crown or haunch bending moment ratio due to the effect of traffic load for different values of height-to-span ratio,
m_{tR} crown or haunch bending moment ratio due to the effect of traffic load for different values of rise-to-span ratio,
M_{cb} crown bending moment due to backfill,
M_{ct} crown bending moment due to traffic load,
M_{hb} haunch bending moment due to backfill,
M_{ht} haunch bending moment due to traffic load,
P_a traffic axial load,
P_D uniformly distributed pressures at the crown due to the soil load,
P_L uniformly distributed pressures at the crown due to the live load,
t_{cb} crown axial force ratio due to backfill,
t_{ct} crown axial force ratio due to traffic load,
t_c crown axial force ratio due to the effect of both backfill and traffic loads,
t_{hb} haunch axial force ratio due to backfill,
t_{ht} haunch axial force ratio due to traffic load,
t_h haunch axial forces ratio due to the

effect of both backfill and traffic loads,
t_{bH} crown or haunch axial force ratio due to the effect of backfill for different values of height-to-span ratio,
t_{bR} crown or haunch axial force ratio due to the effect of backfill for different values of rise-to-span ratio,
t_{tH} crown or haunch axial force ratio due to the effect of traffic load for different values of height-to-span ratio,
t_{tR} crown or haunch axial force ratio due to the effect of traffic load for different values of rise-to-span ratio,
T_{cb} the crown axial force due to backfill,
T_{ct} crown axial force due to traffic load,
T_{hb} haunch axial force due to backfill,
T_{ht} haunch axial force due to traffic load,
S bridge span,
W weight of the fill above the conduit,
H/S the height of cover-to-span ratio,
R/S rise-to–span ratio,
ν Poisson's ratio of soil,
σ_L equivalent uniform distributed load at the crown level,
α_D dead loads factor,
α_L live loads factor,
γ soil density, and
ϕ angle of internal friction of soil.

References

[1] I.F. Christie, "Economic and Technical Aspects of Embankments Reinforced with Fabric", Second International Conference on Geotextile, Slopes and Embankments, pp. 659-664, Las Vegas, U.S.A. (1982).

[2] N. John, P. Johnson, R. Ritson and D. Petley, "Behavior of Fabric Reinforced Soil Walls", Second International Conference on Geotextile, Walls and Foundations, pp. 569-573, Las Vegas, U.S.A. (1982).

[3] C.J.F.P Jones, "Practical Construction Techniques for Retaining Structures Using Fabrics and Geogrids", Second International Conference on Geotextile, Walls and Foundations, pp. 581-585, Las Vegas, U.S.A. (1982).

[4] R.K. Rowe, "The Analysis of an Embankment Constructed on a Geotextile", Second International Conference on Geotextile, Slopes and Embankments, pp. 677-682, Las Vegas, U.S.A., (1982).

[5] S.C. Shrestha and G.R. Bell, "A Wide Strip Tensile Test of Geotextile", Second International Conference on Geotextile, Properties and Tests, pp. 739-744, Las Vegas, U.S.A. (1982).

[6] G. Abdel-Sayed and Y. Girges, "Stability of Soil-Steel Bridges", Canadian Journal of Civil Engineering, Vol. 19 (3), pp. 463-468 (1992).

[7] G. Abdel-Sayed, B. Bakit and L.G. Jaecer, "Soil-Steel Bridges", McGraw-Hill, Inc., New York (1993).

[8] B. Bakit, "Soil-Steel Structure Response to Live Load", Journal of Geotechnical Engineering Division, ASCE, pp. 779-798 (1981).

[9] J.M. Duncan, "Behavior and Design of Long-Span Metal Culverts" Journal of Geotechnical Engineering Division, ASCE, Vol. 105, GT3, pp. 399-418 (1979).

[10] Ontario Highway Bridge Design Code, OHBDC "Soil-Steel Bridges", McGraw-Hill, Inc., New York, Chapter 5, pp 135-151 (1993).

[11] American Association of State Highway and Transportation Officials, AASHTO "Soil-Steel Bridges", McGraw-Hill, Inc., New York, Chapter 5, pp 158-165 (1993).

Received May 25, 2003
Accepted September 7, 2003